Method to Compare Fission-to-Scattering Ratios using Uranium-238

Adam M. Daskalakis[1][*], *Amanda M.* Lewis[1], *Michael J.* Rapp[1], *Devin P.* Barry[1], *Ezekiel J.* Blain[2], *Robert C.* Block[2], and *Yaron* Danon[2,]

[1]Naval Nuclear Laboratory, P.O. Box 1072, Schenectady, New York 12301-1072
[2]Rensselaer Polytechnic Institute, Gaerttner LINAC Center, Troy, New York 12180

Abstract. A novel method was developed to separate the ^{238}U fission contribution measured in quasi-differential time-of-flight scattering experiments in order to isolate the elastic and inelastic events. Pulse height distributions from in-beam measurements were used to generate response functions, which were used to reconstruct the ^{238}U prompt fission neutron spectra. This method was validated by reconstructing the measured ^{252}Cf spontaneous fission pulse height distribution. Monte Carlo calculations were used to model the experiment. Good agreement was observed between the measured and calculated ^{238}U fission contribution.

1 Introduction

The Rensselaer Polytechnic Institute (RPI) high-energy quasi-differential neutron scattering (HES) system collects data generated by the deposition of energy from neutrons and gamma-rays emanating from a sample-of-interest placed in a pulsed neutron beam. The system was configured to measure neutrons with energies between ≈ 0.5 and 20 MeV. Data from these measurements were compared to evaluated nuclear data libraries using Monte Carlo simulations. Observed differences between measured data and Monte Carlo calculations have been used by evaluators to constrain their models [1]. Past measurements using the HES system included graphite (carbon) [2], beryllium [3], molybdenum [3], zirconium [4], ^{238}U [5], iron [6], lead [7], and copper [8].

This study revisits previously measured ^{238}U data to describe a novel approach that separates the fission contribution from other reaction channels. This method relies on in-beam response functions and builds on previously described techniques used to quantify the elastic-only contribution [6, 9]. Results are compared with MCNP [10] simulations to demonstrate proof-of-principle.

2 Background

2.1 RPI LINAC

Experiments were conducted at the Gaerttner Linear Accelerator (LINAC) Center at RPI. The LINAC generated a pulsed electron beam that struck a neutron-producing tantalum target, and through Bremsstrahlung generation and subsequent photoneutron reactions generated a pulsed neutron beam. Neutrons that escaped the tantalum target in the HES system's direction traversed a series of evacuated and collimated flight tubes that ensured the beam diameter was ≈ 7.62 cm at the scattering sample location.

Beam monitors were used to correct for fluctuations in the neutron beam's intensity. They were positioned on an independent flight path at ≈ 9 m from the tantalum target and collected data throughout the measurement.

2.2 HES System

The HES system is comprised of eight detectors positioned around a scattering sample at angles based on observed discrepancies between evaluated nuclear data libraries [2]. Each detector featured a 12.7 cm diameter by 7.62 cm thick ELJEN Technologies EJ-301 liquid scintillator directly coupled to a 12.7 cm diameter Photonis model XP4572/B photomultiplier. Negative high voltage was supplied by a CAEN power supply, model 1733N. Analog signals generated by scintillation light were sent to an Agilent-Acqiris AP240 8-bit data acquisition (DAQ) board via RG-58 coaxial cables [11]. The DAQ maximum sampling rate was 1 GHz which allowed for 1 ns data collection intervals, and each digitized waveform captured a sequence of 120 1-ns samples per event.

2.3 Data Analysis

A series of calculations were performed on each event to classify it as either a neutron or gamma-ray. The event's pulse height, which represents the area under a pulse after baseline subtraction, was also extracted during those calculations. Neutron pulse height distributions are the basis for response functions and the analysis explained in the subsequent sections. Gamma-ray pulse heights were used with a gamma-ray misclassification correction, *GMC*, which corrected the neutron data for gamma-ray events erroneously classified as neutrons. The *GMC* is

---

[*]e-mail: Adam.Daskalakis@unnpp.gov

proportional to pulse height, *j*, with largest correction occurring at low pulse heights [9].

The neutron time-of-flight (TOF) method was used to convert a neutron's recorded time-bin, *i*, to energy, E_i. This relationship is shown in Equation 1.

$$E_i = m_n c^2 \left(\frac{1}{\sqrt{1 - (\frac{L}{c \cdot i})^2}} - 1 \right) \quad (1)$$

where,

$m_n c^2$	=	Neutron rest mass.
L	=	Total flight path for in-beam measurements, 30.07 m.
c	=	The speed of light in vacuum.
i	=	Neutron time-of-flight.

2.4 Response Functions

Detector in-beam measurements collected data from a single detector placed in the neutron beam path at ≈30 m from the tantalum target without the presence of a scattering sample. To approximate a mono-energetic neutron beam only data in a narrow energy bin, $E_i \pm dE_i$, were analyzed. Vectors, or histograms, of pulse heights were generated from that data. These distributions are referred to as energy-dependent response functions, or R_{E_i}. Each response function has a unique distribution based on the incident neutron energy. All response functions set dE_i to 2.5% of E_i, i.e., 1 ± 0.025 MeV. The limited energy range also allows for the approximation that neutron flux does not vary much, and was considered constant throughout this energy bin.

Figure 1 displays three response functions for incident neutron energies of 1.0 ± 0.025, 1.5 ± 0.038, and 2.0 ± 0.05 MeV. All data were measured by a single detector.
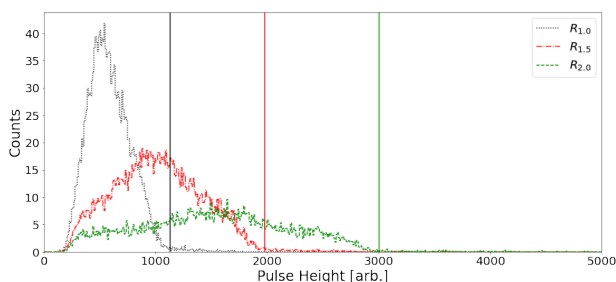

Figure 1. Three response functions generated from in-beam data for incident neutrons at 1.0 ± 0.025, 1.5 ± 0.038, and 2.0 ± 0.05 MeV. The vertical lines represent the end-point locations for each of the response functions. Data were grouped and averaged over 50 pulse height bins.

Figure 1 also shows that the maximum pulse height that contributes to the response function increases with incident neutron energy. This location is referred to as the response function end-point, and its position was determined by traversing the pulse height distribution until ≈99.5% of all pulses contributing to the histogram were summed. A

third-order polynomial was fit to each response function's end-point, which is displayed in Figure 2.
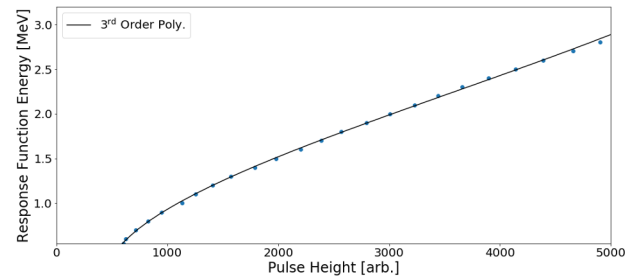

Figure 2. Pulse height end-points for each response function with respect to incident neutron energy. A third-order polynomial fit to these points was used to calculate the maximum pulse height achievable by different scattering reactions based on the incident neutron energy.

For a given incident neutron energy, only neutrons from fission events have energies in excess of elastic scattering. Therefore, to isolate the fission contribution at E_i an end-point corresponding to an elastically scattered neutron with energy $\leqq E_i$ was calculated using the aforementioned polynomial. The fission shape was then normalized to the region above the end-point bin, discussed in 4.2, to ascertain the fission neutron contribution.

3 ^{252}Cf Measurement and Analysis

To demonstrate that response functions can successfully reconstruct the ^{238}U prompt fission neutron spectra (PFNS) pulse height distribution from measured HES data, a proof-of-concept calculation was performed using data previously measured from a ^{252}Cf source to quantify the *GMC* [9].

A series of response functions were generated to cover the range of fission neutron energies that were measured by the HES detectors. Response function pulse height distributions were generated for energies between 0.55 and 20 MeV in 0.1 MeV increments. Each response function was weighed by the corresponding ENDF/B-VIII.0 [12] ^{252}Cf PFNS neutron yield and summed. This resulted in a reconstructed spontaneous fission pulse height distribution from the ^{252}Cf source, $R_{\chi_{s.f.}^{252}}$, as shown in Equation 2.

$$R_{\chi_{s.f.}^{252}} = \sum_{k=0.55}^{20} R_{E_k} \chi_{s.f.}^{252}(E_k) \quad (2)$$

where,

$R_{\chi_{s.f.}^{252}}$	=	Reconstructed spontaneous fission neutron pulse height distribution from coupled χ^{252} and in-beam response functions.
$\chi_{s.f.}^{252}(E_k)$	=	Spontaneous fission PFNS distribution for neutrons at energy E_k.
R_{E_k}	=	The detector's response function at energy E_k.
E_k	=	Fission neutron energy at *k*.

$R_{\chi_{s.f.}^{252}}$ was area normalized to the measured ^{252}Cf pulse height data and is displayed in Figure 3, which shows good agreement between the measured ^{252}Cf data and $R_{\chi_{s.f.}^{252}}$. The only source of uncertainty presented here comes from counting statistics associated with the ^{252}Cf and background measurements. Additional sources of uncertainty can be attributed to response functions' pulse height distributions, detector efficiencies, and experimental setup; however, those sources were not characterized.
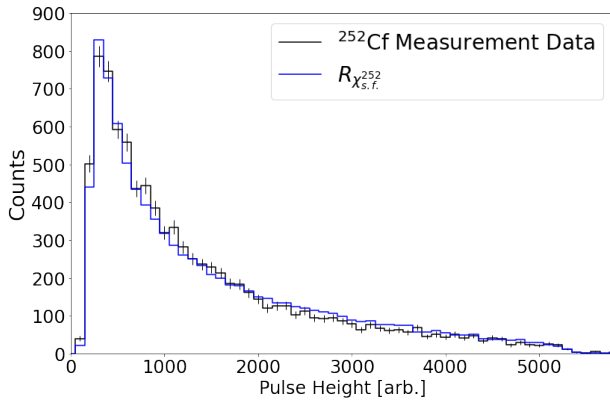

Figure 3. $R_{\chi_{s.f.}^{252}}$ was area normalized to the measured ^{252}Cf pulse height distribution. Counting statistics were the only source of uncertainty included for this analysis. Data were grouped and averaged over 100 pulse height bins.

Despite the low counts, in-beam response functions and $R_{\chi_{s.f.}^{252}}$ obtained from ENDF/B-VIII.0 could be used to reconstruct the measured ^{252}Cf pulse height distribution. This forms the basis for reconstructing the ^{238}U energy dependent PFNS pulse height distribution, or $R_{E_i^{238}}$.

4 Separating Fission from Scattering in ^{238}U

The ^{238}U measurement and analyses were previously performed with the intent to constrain models used to help generate evaluated nuclear data libraries. Experiment conditions, results, and findings are documented in [1, 5, 9]. ^{238}U data from a single detector, along with the corresponding in-beam response functions, were reanalyzed. During the ^{238}U measurement that detector was positioned at 130 relative to the incident neutron beam. ^{238}U results using the methods described above are detailed in the subsequent sections.

4.1 Generating ^{238}U Fission Pulse Height Distribution

The ^{238}U scattering measurement differed from the ^{252}Cf static measurement in several ways. First, the open beam, or time-dependent background, pulse height contribution was removed. For quasi-differential measurements the time-independent room background was negligible. Second, the ^{252}Cf sample was considered a point source, and

neutron transmission through the low mass fission chamber was neglected. In contrast, both incident and fission neutrons had to traverse part of the ^{238}U sample. An energy-dependent correction was applied to response functions and is included in Equation 3. This correction calculates the fraction of fission neutrons that did not interact with the ^{238}U sample. The depth where fission was modeled corresponds to where 50% of interactions occurred in the ^{238}U sample. This depth varied based on the incident neutron's energy, E_i.

$$R_{E_i}^{238} = \sum_{k=0.55}^{20} \chi_{E_i}^{238}(E_k) R_{E_k} \left(1 - e^{-Nx(E_i)\sigma_t(E_k)}\right) \quad (3)$$

where,

$R_{E_i}^{238}$	=	Reconstructed ^{238}U fission neutron pulse height distribution for incident neutron energy E_i.
$\chi_{E_i}^{238}(E_k)$	=	Probability of a fission neutron with energy E_k. The ^{238}U PFNS distribution was calculated based on incident neutron energy E_i.
R_{E_k}	=	Response function for fission neutron at energy E_k
N	=	^{238}U sample number density.
$x(E_i)$	=	Depth where 50% of interactions occurred within the ^{238}U sample at energy E_i. The ^{238}U thickness was 0.979 cm.
$\sigma_t(E_k)$	=	The ^{238}U total cross section at E_k.

The ^{238}U energy bins analyzed were set dE_i to 2.5% of E_i, mimicking the energy bins used to generate in-beam response functions. Additional effort was made to include the contribution of fission neutrons from times outside the energy bin being analyzed, i.e., high-energy fission neutrons from incident neutron energies $< E_i$ and vise versa, which resulted in a minor correction.

4.2 Calculating the Fission Contribution

After $R_{E_i}^{238}$ was generated an end-point corresponding to elastically scattered neutrons at energy E_i to the detector at 130 degrees was calculated using the polynomial presented in Figure 2. For incident 1.7 MeV neutrons this corresponded to a pulse height of $\approx$2200 and $R_{E_i}^{238}$ was area normalized to the pulse height data above this location. After normalization, the fission neutron ratio was calculated by taking the ratio of the reconstructed ^{238}U fission neutron pulse height distribution relative to all measured neutrons in a given energy-bin.

Figure 4 shows the measured ^{238}U pulse height distribution and $R_{1.7}^{238}$, the reconstructed ^{238}U fission neutron pulse height distribution for incident 1.7 MeV neutrons. $R_{1.7}^{238}$ was area normalized to the measured ^{238}U region above the 1.7 MeV elastically scattered end-point.
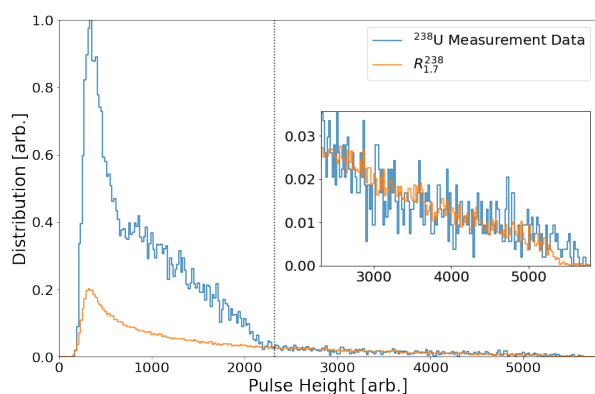
Figure 4. Measured pulse heights for incident 1.7 MeV neutrons on the ^{238}U sample. $R_{1.7}^{238}$ was normalized to the measured data, which was peak-normalized to unity. The vertical dotted line represents the elastic scattering end-point location and the inset plot shows the region where normalization occurred. Data were grouped and averaged over 50 pulse height bins.

The measured fission neutron ratios were compared with MCNP simulations that modeled the ^{238}U quasi-differential measurement. ENDF/B-VIII.0 , JEFF-3.3 , and JENDL-4.0 ^{238}U evaluations were compared with the measured data by only varying the evaluation used to model the ^{238}U reactions. Lastly, at each energy and for each evaluation two separate simulations were performed, with the only difference being the enabling or disabling of the fission contribution from the ^{238}U sample.
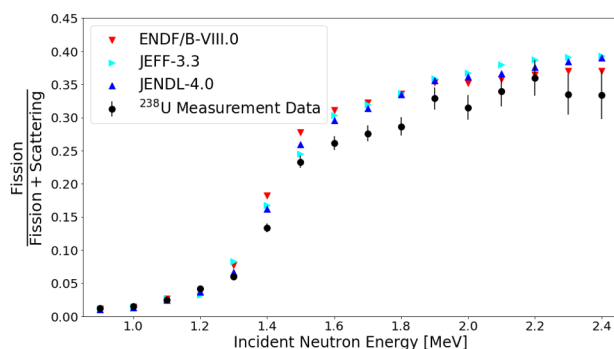

Figure 5. Measured ^{238}U fission neutron ratio compared with the ratio calculated from MCNP simulations. The uncertainties band reflects only the ^{238}U counting statistics. MCNP used the ENDF/B-VIII.0 library for all other cross sections.

The fission ratios from measured data and MCNP simulations have the same general trend. However, the differences observed from 1.4 to 1.8 MeV are large and may warrant additional investigations to determine their origin. Only the ^{238}U statistical uncertainty is reported, and one source for the discrepancies can be attributed to the limited number of counts associated with both response functions and quasi-differential ^{238}U data. Other sources of uncertainty, i,e., systematic, are not included.

5 Conclusion

The method to reconstruct the fission contribution using pulse height information and eliminate it from a

^{238}U scattering measurement was discussed. A proof-of-principle was demonstrated by reconstructing a measured ^{252}Cf PFNS pulse height distribution with in-beam response functions coupled with ENDF/B-VIII.0 prompt fission neutron spectra. This technique was then applied to ^{238}U quasi-differential data in order to separate the fission contribution from scattering reactions. The measured fission contributions were compared with MCNP calculations performed with several libraries, which all showed similar trends.

Eliminating the fission contribution can allow further analysis on anisotropic reactions utilizing the methods discussed herein.

References

[1] R. Capote, A. Trkov, M. Sin, M. Pigni, V. Pronyaev, J. Balibrea, D. Bernard, D. Cano-Ott, Y. Danon, A. Daskalakis et al., Nuclear Data Sheets **148**, 254 (2018)

[2] F. Saglime, Y. Danon, R. Block, M. Rapp, R. Bahran, G. Leinweber, D. Barry, N. Drindak, Nucl. Instrum. Methods Phys. Res., Sect. A **620**, 401 (2010)

[3] Daskalakis, Adam, Blain, Ezekiel, Leinweber, Gregory, Rapp, Michael, Barry, Devin, Block, Robert, Danon, Yaron, EPJ Web Conf. **146**, 11037 (2017)

[4] D. Barry, G. Leinweber, R. Block, T. Donovan, Y. Danon, F. Saglime, A. Daskalakis, M. Rapp, R. Bahran, Nucl. Sci. Eng. **172**, 188 (2013)

[5] A. Daskalakis, R. Bahran, E. Blain, B. McDermott, S. Piela, Y. Danon, D. Barry, G. Leinweber, R. Block, M. Rapp et al., Ann. Nucl. Energy **73**, 455 (2014)

[6] A. Daskalakis, E. Blain, B. McDermott, R. Bahran, Y. Danon, D. Barry, R. Block, M. Rapp, B. Epping, G. Leinweber, Ann. of Nucl. Energy **110**, 603 (2017)

[7] A. Youmans, J. Brown, A. Daskalakis, N. Thompson, A. Weltz, Y. Danon, B. McDermott, G. Leinweber, M. Rapp, AccApp 15, Washington, DC pp. 355–360 (2015)

[8] E. Blain, Y. Danon, D. Barry, B. Epping, A. Youmans, M. Rapp, A. Daskalakis, R. Block, Nuclear Science and Engineering **196**, 121 (2021)

[9] A.M. Daskalakis, Ph.D. thesis, Rensselaer Polytechnic Institute (2015)

[10] C. Werner, J. Bull, C. Solomon, F. Brown, G. McKinney, M. Rising, D. Dixon, R. Martz, H. Hughes, L. Cox et al., *MCNP6.2 Release Notes* (2018)

[11] F.J. Saglime, Ph.D. thesis, Rensselaer Polytechnic Institute (2009)

[12] D. Brown, M. Chadwick, R. Capote, A. Kahler, A. Trkov, M. Herman, A. Sonzogni, Y. Danon, A. Carlson, M. Dunn et al., Nuclear Data Sheets **148**, 1 (2018)